Chaos
An Interdisciplinary Journal of Nonlinear Science

RESEARCH ARTICLE | JULY 12 2024

# Optimal phase-selective entrainment of electrochemical oscillators with different phase response curves

**Special Collection:** Topics in Nonlinear Science: Dedicated to David K. Campbell's 80th Birthday

Jorge Luis Ocampo-Espindola ; Bharat Singhal ; Jr-Shin Li ; István Z. Kiss



*Chaos* 34, 073129 (2024)
https://doi.org/10.1063/5.0205480

# Optimal phase-selective entrainment of electrochemical oscillators with different phase response curves

Cite as: Chaos 34, 073129 (2024); doi: 10.1063/5.0205480
Submitted: 26 February 2024 · Accepted: 25 June 2024 ·
Published Online: 12 July 2024



Jorge Luis Ocampo-Espindola,[1] Bharat Singhal,[2] Jr-Shin Li,[2] and István Z. Kiss[1,a)]

## AFFILIATIONS

[1]Department of Chemistry, Saint Louis University, St. Louis, Missouri 63103, USA
[2]Department of Electrical & Systems Engineering, Washington University in St Louis, St Louis, Missouri 63130, USA

**Note:** This paper is part of the Focus Issue on Topics in Nonlinear Science: Dedicated to David K. Campbell's 80th Birthday.
[a)]**Author to whom correspondence should be addressed:** istvan.kiss@slu.edu

## ABSTRACT

We investigate the entrainment of electrochemical oscillators with different phase response curves (PRCs) using a global signal: the goal is to achieve the desired phase configuration using a minimum-power waveform. Establishing the desired phase relationships in a highly nonlinear networked system exhibiting significant heterogeneities, such as different conditions or parameters for the oscillators, presents a considerable challenge because different units respond differently to the common global entraining signal. In this work, we apply an optimal phase-selective entrainment technique in both a kinetic model and experiments involving electrochemical oscillators in achieving phase synchronized states. We estimate the PRCs of the oscillators at different circuit potentials and external resistance, and entrain pairs and small sets of four oscillators in various phase configurations. We show that for small PRC variations, phase assignment can be achieved using an averaged PRC in the control design. However, when the PRCs are sufficiently different, individual PRCs are needed to entrain the system with the expected phase relationships. The results show that oscillator assemblies with heterogeneous PRCs can be effectively entrained to desired phase configurations in practical settings. These findings open new avenues to applications in biological and engineered oscillator systems where synchronization patterns are essential for system performance.





**Complex systems are often composed of oscillatory units that can entrain to external signals such that the peak times of the oscillations are organized in a given pattern. When the units have distinct, largely nonlinear, dynamics, finding an external waveform that can induce a predetermined sequence (e.g., some units peak together and others at different times) is a tremendously challenging task because each unit responds to the external signal differently. In this study, we demonstrate the entrainment of electrochemical oscillators with different experimental parameters (and, thus, different phase responses) to achieve stable in-phase, anti-phase, and out-phase patterns. Our findings reveal that oscillators with large heterogeneities in their phase responses can be effectively entrained into specified phase patterns. While the entrainment method was tested in electrochemical oscillators, its potential applications extend to biological systems characterized by significant heterogeneous elements with distinct phase response characteristics.**

## I. INTRODUCTION

Large populations of oscillating elements are abundant in nature and engineered systems, ranging from chemical oscillators to the neurons in the brain.[1–3] These populations often require a certain dynamic structure between the elements for the proper functioning of the system. For example, neural activity synchronization is required for perceptual and cognitive functions[4,5] and desynchronization for the transition between perception and the motor response.[6] Any disruption of these self-organizing structures can result in pathological disorders;[7–9] for instance, increased neuronal synchrony has been linked with motor dysfunctions in Parkinson's disease.[10,11] Given these practical applications, it is important to design external stimuli that can obtain the desired synchronization structures in heterogeneous oscillator populations, all the while being robust to experimental noise and without disrupting the local oscillatory dynamics.

Feedback-based techniques have been shown to be effective in regulating oscillator populations in both theory and experiments.[12–14] This includes tuning the phase relationships between the oscillators,[15] the desynchronization of oscillator populations,[13,16,17] cluster formation,[16,18] and the formation of chimera states.[19–21] The robustness of these techniques to experimental uncertainties can be attributed to the intrinsic nature of feedback, which facilitates disturbance rejection. Nonetheless, implementations require real-time measurement of oscillator units, and determining feedback parameters often hinges on certain assumptions regarding population dynamics, such as similar oscillator parameters or infinite oscillator populations.

In addition to feedback approaches, open-loop methods have also been investigated for applications where real-time feedback acquisition is unfeasible. Open-loop applications were developed for control of quantum systems, where robust manipulation of spins for generic many-body systems was achieved.[22,23] Similar open-loop techniques were also directed toward desynchronizing oscillator populations with various kinds of pulses, including single pulse design,[24] double-pulse design,[25,26] bi-polar double pulse,[27] and a combination of the pulse train followed by a single pulse.[28,29] These designed pulses often lacked optimality, necessitating the integration of optimal control theory since applying large external signals can potentially be harmful to clinical applications such as deep-brain stimulation. The optimal control techniques were applied to design optimal time or energy stimuli for a single oscillator,[30,31] the population of oscillators,[32,33] and the optimal entertainment of neuronal populations.[34,35]

Despite their effectiveness, homogeneity in the oscillator populations is a common assumption for the underlying theory behind these methods, which leverages phase-model descriptions of oscillator populations. Specifically, the oscillators are typically assumed to have identical PRC. These PRCs characterize the effect of input on oscillation phases and are often nonidentical between oscillators. Some common examples of heterogenous PRC oscillator populations include cortical pyramidal neurons,[36,37] mitral cells in the olfactory bulb,[38] and circadian oscillator in Gonyaulax.[39] With electrochemical oscillators, a wide range of PRCs were experimentally measured;[40] for example, for oscillators close to a Hopf bifurcation, the PRC consisted of only a single harmonic component, but further away from the bifurcation point, PRCs with dominant higher harmonics were observed.

Oscillators with different PRCs can challenge the applicability of current techniques. For example, a versatile phase-selective entertainment procedure was proposed that used natural frequency heterogeneities to engineer a frequency synchronized ensemble with a pre-specified phase pattern.[41] When oscillators have both different frequencies and PRCs, each oscillator would entrain differently to the same global signal, and, thus, finding waveforms for specified phase patterns is a difficult task. Similarly, waveforms for entrainment to given phase patterns are often desired to have low power to eliminate undesirable side effects of using large signals and also to ensure that weak forcing approximations, which are often used in theoretical frameworks, remain valid. Therefore, there is a need to extend the applicability of synchronization engineering techniques to address the entrainments of oscillators with different PRCs using low-power signals.

In our previous work,[42] an optimal input design framework was proposed to entrain heterogeneous PRC oscillators in a prespecified configuration. Starting with a phase-model description of the oscillators that have distinct natural frequencies and PRCs, waveforms were constructed that not only entrained the oscillators in a given phase configuration but also addressed optimality in terms of signal power and entrainment rate. This was achieved by elucidating the complex synchronization engineering task into a convex optimization problem. However, despite the theoretical foundations, the technique was only validated using simple phase oscillators, and, thus, important questions remained open related to the extent to which the method can be applied to systems beyond phase oscillators, e.g., multivariable ordinary differential equations (ODEs) or experiments.

In this paper, we leverage the optimal phase-selective entrainment technique introduced in our previous work[42] to induce the desired synchronization structures in an array of heterogeneous (nonidentical PRC) electrochemical oscillators. Specifically, we validate the theoretical framework introduced in Ref. 42 through experiments with oscillatory electrochemical reactions as well as numerical simulations with a kinetic ODE model. The optimality of our method and its robustness against population heterogeneity is demonstrated using a comparative analysis with the previous phase assignment technique, which used averaged PRCs.[41] This allows us to elucidate how the performance of entrainment signals designed with averaged PRCs differs from those with individualized PRCs.

## II. MATERIALS AND METHODS

### A. Phase models

We consider a $m$-dimensional ($m \geq 2$) limit-cycle oscillator described by a smooth ordinary differential equation,

$$\dot{x} = f(x, u), \qquad x(0) = x_0, \tag{1}$$

where $x \in \mathbb{R}^m$ is the system state and $u \in \mathbb{R}$ is the external input. For a weak $u(t)$ such that the system remains in the neighborhood of the unforced limit-cycle, the evolution of the original $m-$dimensional system can be captured by a reduced one-dimensional system, known as the phase model. These phase models can be evaluated analytically using the phase reduction theory[43] and can also be estimated experimentally for a system with unknown dynamics.[44] By applying the phase reduction theory, the dynamics of an ensemble of oscillators can be described by

$$\dot{\theta}_j(t) = \omega_j + Z_j(\theta_j)u(t), \qquad j = 1, \ldots, N, \tag{2}$$

where $\theta_j, \omega_j$, and $Z_j(\theta_j)$ are the phase, natural frequency, and PRC of oscillator $j$. A PRC is a $2\pi$-periodic function that characterizes the response of the oscillator phase to weak inputs and can be determined experimentally or numerically.[44–47]

### B. Optimal phase-selective entrainment

Here, we describe the key principles of the optimal phase-selective entrainment technique introduced in Ref. 42 that decodes the complex task of synchronization engineering into a convex optimization problem. The objective of our technique is to design an external periodic input of a given frequency $\Omega$ that can entrain a

population of heterogeneous oscillators at phases $\varphi_1^*, \ldots, \varphi_N^*$ while having minimum power. To begin, we take the oscillator population of (2) and consider their averaged phase model description,

$$\dot{\varphi}_j = \Delta\omega_j + \Lambda_{u,j}(\varphi_j), \qquad j = 1, \ldots, N, \tag{3}$$

where $\varphi_j$ and $\Delta\omega$ are the phase difference and frequency difference between the oscillator $j$ and the periodic forcing $u$, respectively; $\Lambda_{u,j}(\varphi_j) = \frac{1}{2\pi}\int_0^{2\pi} Z_j(\theta + \varphi_j)u(\theta)d\theta$ is the interaction function of oscillator $j$ that characterizes the average effect of input over one cycle. During entrainment, the phase difference between the oscillators and input becomes constant, which results in $\dot{\varphi}_j = 0$ for $j = 1, \ldots, N$. Thus, to entrain the oscillator $j$ at $\varphi_j^*$, the interaction function $\Lambda_{u,j}$ must satisfy

$$\begin{aligned} \Delta\omega_j + \Lambda_{u,j}(\varphi_j^*) &= 0, \\ \Lambda'_{u,j}(\varphi_j^*) \le 0, \qquad j &= 1, \ldots, N, \end{aligned} \tag{4}$$

where $\Lambda'_{u,j}$ denotes the first-order derivative of $\Lambda_{u,j}$, and the second condition is added to ensure stable entrainment.

### 1. Convex optimization formulation for control design

For the oscillator ensemble, each PRC (known) is a $2\pi$-periodic function and, hence, can be approximated using Fourier series. Let $a_{0,j}, \{a_{n,j}, b_{n,j}\}_{n=1}^{r_j}$ be the Fourier coefficient of $Z_j(\theta)$ and $i$ be the oscillator index with the largest number of Fourier harmonics, i.e., $r_i = \max(r_1, \ldots, r_N)$. Similarly, we denote $c_0, \{c_n, d_n\}_{n=1}^{r}$ and $f_{0,j}, \{f_{n,j}, f_{n,j}\}_{n=1}^{\min(r,r_j)}$ as the input and $\Lambda_{u,j}$ Fourier coefficients, which are to be determined ($r = r_i$). As a result of this Fourier decoding, the optimal interaction function of oscillator $i$ can be obtained by solving the convex optimization problem,

$$\begin{aligned} \min_{\boldsymbol{y}} \quad & \frac{1}{2}\boldsymbol{y}^T Q \boldsymbol{y}, \\ \text{s.t.} \quad & A\boldsymbol{y} = \boldsymbol{b}, \\ & G\boldsymbol{y} \le \boldsymbol{h}, \end{aligned} \tag{5}$$

where $\boldsymbol{y} = [f_{0,i}, f_{1,i}, g_{1,i}, \ldots, g_{r,i}]$, $\boldsymbol{b} = [-\Delta\omega_1, \ldots, -\Delta\omega_N]$, $Q \in \mathbb{R}^{(2r+1)\times(2r+1)}$ is a diagonal matrix with non-negative entries that depends on oscillator $i$ PRC coefficients, and the matrices $A, G \in \mathbb{R}^{N\times(2r+1)}$ satisfy $(A)_j\boldsymbol{y} = \Lambda_{u,j}(\varphi_j^*)$ and $(G)_j\boldsymbol{y} = \Lambda'_{u,j}(\varphi_j^*)$, with $(A)_j$ and $(G)_j$ denoting the $j$th row of the matrix $A$ and $G$; $\boldsymbol{h} = [h_1, \ldots, h_N]$ ($h_j \le 0$) is added to ensure a faster rate of convergence to the fixed points $\varphi_j^*, j = 1, \ldots, N$. The objective function and the constraints correspond to input power and the entrainment conditions, respectively. After obtaining $\boldsymbol{y}$, the optimal input can be determined from the relation between the interaction function, input, and PRC (see Ref. 42 for more details). Other objectives, for example, fast entrainment, can also be achieved by modifying the objective criteria to $\boldsymbol{y}^T G^T G \boldsymbol{y}$ to maximize the slope of the interaction function.

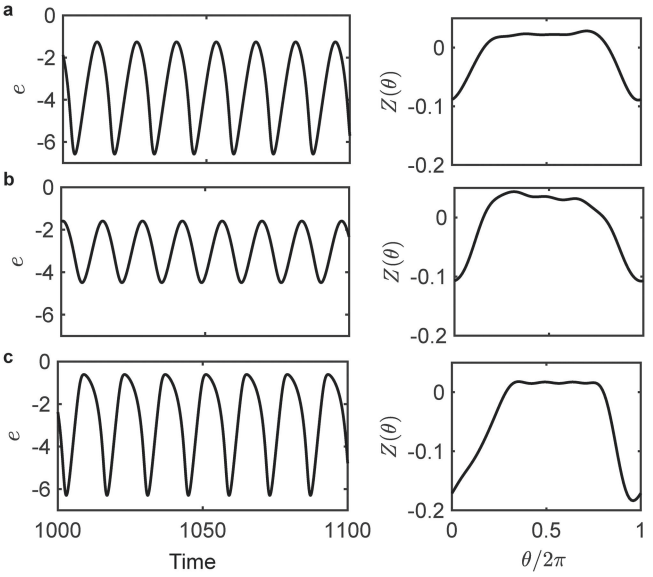


**FIG. 1.** Model simulations: electrode potential $e(t)$ and the estimated PRC of the electrochemical oscillator model for different values for circuit potential $V$, resistance $R$, and $\Gamma$. (a) $(V_1, R_1, \Gamma_1) = (15, 20, 10^{-2})$. (b) $(V_2, R_2, \Gamma_2) = (15, 25, 10^{-2})$. (c) $(V_3, R_3, \Gamma_3) = (24.9, 20, 8.5 \times 10^{-3})$.

## C. Numerical simulations

We consider a set of oscillators describing nickel electrodissolution reaction in sulfuric acid with the dynamics equations,[48]

$$\begin{aligned} \frac{de_j}{dt} &= \frac{V_j + u(t) - e_j}{R_j} - \left[\frac{C_h \exp(0.5e_j)}{1 + C_h \exp(e_j)} + a\exp(e_j)\right](1 - \nu_j), \\ \Gamma_j \frac{d\nu_j}{dt} &= \frac{\exp(0.5e_j)}{1 + C_h \exp(e_j)}(1 - \nu_j) - \frac{bC_h \exp(2e_j)}{cC_h + \exp(e_j)}\nu_j, \end{aligned} \tag{6}$$

where the state variables $e_j$ and $\nu_j$ denote the electrode potential and the surface coverage of the passivating oxide species of the $j$th oscillator, and $u(t)$ denotes the common input to the oscillators. The parameters $C_h = 1600$, $a = 0.3$, $b = 6 \times 10^{-5}$, and $c = 10^{-3}$ are identical for different oscillators, while the circuit potential, $V_j$, resistance, $R_j$, and $\Gamma_j$ are varied to introduce heterogeneity in oscillator frequencies and PRC. The heterogeneous PRCs of three oscillators corresponding to $(V_1, R_1, \Gamma_1) = (15, 20, 10^{-2})$, $(V_2, R_2, \Gamma_2) = (15, 25, 10^{-2})$, and $(V_3, R_3, \Gamma_3) = (24.9, 20, 8.5 \times 10^{-3})$ are displayed in Fig. 1. These PRCs are determined by applying narrow pulses to the electrode potential and measuring the oscillation phase shift.

## D. Experiments

The experiments were performed in a standard three-electrode electrochemical cell. An array of 1 mm nickel wires (W), a platinum rod counter (C), and a $Hg/Hg_2SO_4$/sat. $K_2SO_4$ (R) reference electrodes were used. The electrodes were immersed in an electrolyte solution of 3 m sulfuric acid and kept at 10° C. The offset

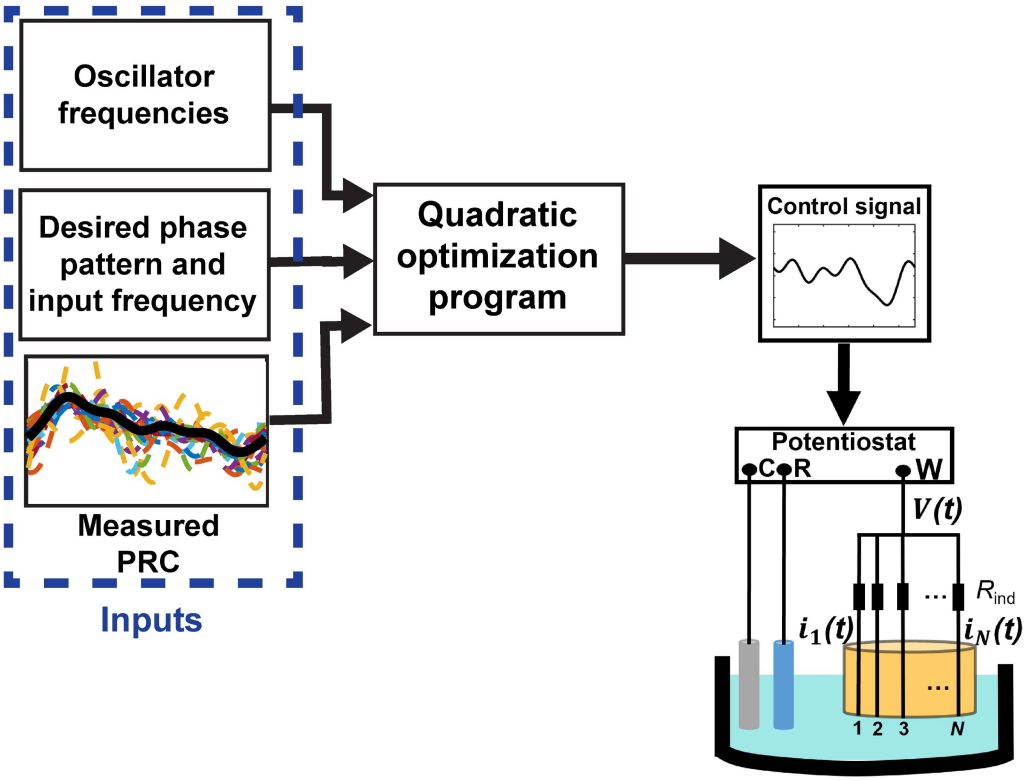


**FIG. 2.** Schematic of the open-loop control design for oscillatory electrochemical reactions. The inputs for the proposed technique consisted of (i) the natural frequency of the oscillators, (ii) the desired phase pattern and the frequency of periodic forcing, and (iii) the phase response curves. The forcing signal $u(t)$ is designed by plugging in the parameters to optimization problem (5). The estimated input is then applied by superposing it to the circuit potential offset, $V_0$, i.e., $V(t) = V_0 + u(t)$. C: counter electrode, R: reference electrode, and W: working electrode array. The current, $i_j(t)$ ($j = 1, \ldots, N$, where $N$ is the number of units), generated by the electrodissolution process is measured by the potential drop across resistance $R_{ind}$.

circuit potential ($V_0$) was set by the potentiostat (GillAC) and the control signal $u(t)$ was superimposed on the offset circuit potential $[V(t) = V_0 + u(t)]$. When an individual resistance ($R_{ind}$) is attached to each working electrode, the nickel dissolution exhibits oscillatory behavior through a Hopf bifurcation.[49]

In the experiments, three offsets of the circuit potentials ($V_0 = 1090, 1150$, and 1250 mV) and two different values of the individual resistance ($R_{ind} = 1$ and 1.5 kΩ) were used to induce heterogeneity in the oscillators. Notice that because of different individual resistances, the Hopf point (onset of oscillations) also changed and, therefore, the oscillation frequency.[50] To induce a more relaxational waveform character, the offset circuit potential was increased to values further away from the Hopf bifurcation.[40,51]

Due to inherent heterogeneities in the nickel wires, including variations in the composition, size, and surface conditions such as oxide film layer thickness and localized corrosion, the electrochemical oscillators exhibited slight discrepancies in the natural frequencies. To account for such variation in the frequencies, the experiments reported in this work involved selecting the natural frequency of two (or four) oscillators from an array of 25. The frequency difference was kept in the interval from 0.125 to 0.5 rad/s. A pseudorandom sequence of narrow pulses was applied to the offset circuit potential during each experiment at different parameter conditions ($V_0$ and $R$). Each of these pulses had a magnitude of 200 mV and a duration of 0.05 s. Subsequently, we determined the corresponding PRC for each oscillator[41,52] and calculated an average PRC derived from 25 oscillators.

The schematic of the experimental implementation of the open-loop control is shown in Fig. 2. Our initial step involves measuring both the oscillation frequency and the PRC of the oscillator populations. These measured parameters, along with the desired phase pattern, are fed into the optimization block. The operations of the optimization block are (i) the approximation of measured PRCs with Fourier series with the desired accuracy; (ii) the construction of matrices $A$ and $G$, and the vector $\boldsymbol{b}$ using the approximated PRC coefficients, oscillator frequencies, input frequency, and the desired entertainment phases (entries of $\boldsymbol{h}$ are kept identical for all the oscillators); and (iii) the generation of optimal input by solving (5) using an optimization solver. The synthesized signal is then applied through a superposition operation, effectively modulating the circuit potential offset across all oscillators.

## III. RESULTS AND DISCUSSIONS

### A. Numerical simulations

In this section, we first illustrate the optimality and robustness to PRC variations in the proposed phase assignment technique via numerical simulations performed on a pair of electrochemical oscillators (6) (Fig. 3). Subsequently, we demonstrate phase-selective entrainment of four oscillators (Fig. 4).

#### 1. Entrainment of an oscillator pair

In Fig. 3, we consider three pairs of oscillators, each with distinct levels of heterogeneity in their PRC and compare the proposed technique with the method introduced in Ref. 41, hereby referred to as the baseline method. The PRCs of the first pair are identical [Fig. 1(a)], those of the second pair exhibit some heterogeneity [Figs. 1(a) and 1(b)], while the PRCs of the third pair display more pronounced heterogeneity [Figs. 1(a) and 1(c)].

**Case 1 (Identical PRC):** We proceed to entrain the first pair of oscillators with natural frequencies $(\omega_1, \omega_2) = (0.4505, 0.4536)$ rad/s in an in-phase configuration with an input of frequency $\Omega = 0.4521$ rad/s using the proposed method by taking $(\varphi_1^*, \varphi_2^*) = (\pi/2, \pi/2)$. To this end, we first fit the oscillator PRC using a Fourier series of six harmonics and construct the matrices $A$, $G$, and $Q$ using the fitted Fourier coefficients and the desired entrainment phases.

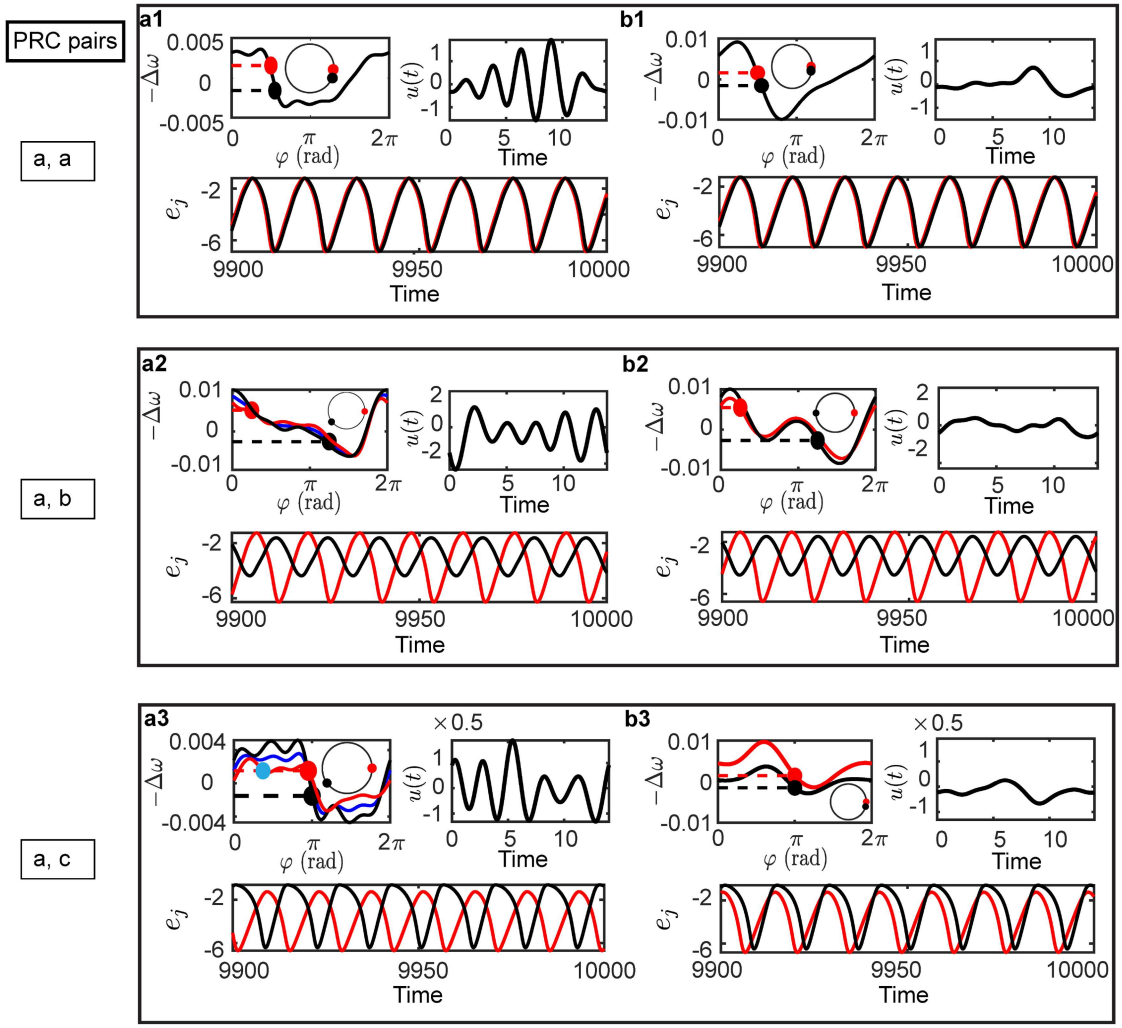


**FIG. 3.** Numerical simulations: A comparison of the optimality and robustness again PRC heterogeneity of the proposed technique [(b1)–(b3)] with the baseline method [(a1)–(a3)]. The top-left, top-right, and bottom figures of each panel depict the designed interaction function (with inset showing phases on the unit circle), control input, and the time series of the electrode potential, where the red and black colors correspond to the slower and faster oscillators, respectively. (a1) and (b1), (a2) and (b2), and (a3) and (b3) correspond to three different pairs of the PRC depicted in Fig. 1. The blue line in (a2) and (a3) shows the interaction function corresponding to the mean PRC of two oscillators. The stable entrainment phases are the points where the horizontal line $(-\Delta\omega)$ intersects the interaction function at the negative slope.

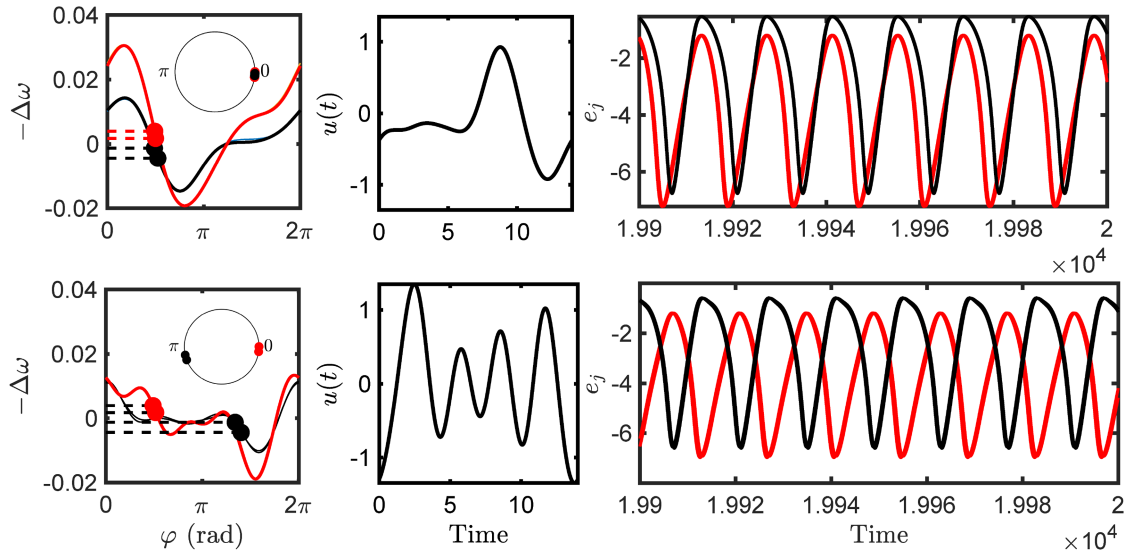


**FIG. 4.** One-cluster (top) and two-cluster (bottom) state with four oscillators. Left to right: interaction function (inset: phases on the unit circle), control input, and the electrode potential time series. The red (black) color denotes the slower (faster) oscillators, where oscillators having identical PRC are represented by the same color.

The interaction function is then obtained by solving the optimization program (5) where the entries of vector $h$ are set as $-0.01$. The designed interaction function, corresponding control input, and the resulting electrode potential waveform are shown in the upper-left, upper-right, and lower sections of panel b1 in Fig. 3, where the slower (faster) oscillator is denoted by the red (black) color. Now, we repeat the same task of in-phase entrainment using the baseline method, with the results shown in Fig. 3(a1). The principle idea behind the baseline method is to first design a step-like phase interaction function that passes through the entrainment phases with a negative slope and then approximate this function with a Fourier series to obtain the interaction function and the input. We find a substantial sevenfold input power reduction, decreasing from 0.61 to 0.09, achieved by the proposed technique compared to the baseline approach. The difference between the desired and observed phase difference remains consistently small for both methods (0.09 and 0.18 rad for the updated and baseline, respectively). Note that the input power and the error are defined as $\frac{1}{2\pi}\int_0^{2\pi} u^2(\theta)d\theta$ and $\sqrt{\left(\Delta\theta_{designed}-\Delta\theta_{observed}\right)^2}$, respectively, where $\Delta\theta_{designed}$ and $\Delta\theta_{observed}$ denote the desired and observed phase differences between the oscillators.

**Case 2 (Marginally heterogeneous PRC):** Now, we consider a pair of marginally distinct PRC oscillators with $(\omega_1, \omega_2) = (0.4505, 0.4587)$ rad/s and entrain them in an anti-phase configuration by taking $(\varphi_1^*, \varphi_2*) = (\pi/4, 5\pi/4)$ using an input of $\Omega = 0.456$ rad/s. We repeat a similar procedure as in the identical PRC case to construct the interaction function (shown in the upper-left image in Fig. 3(b2)). The corresponding control input and the electrode potential waveforms are shown in the upper-right and bottom sections, respectively. As the baseline method assumes the oscillators to have identical PRCs, we employ the mean PRC to design the interaction function for comparative analysis. The mean interaction function is depicted by the blue line in the upper-left figure of panel a2, where red and black lines denote the interaction functions associated with the true oscillator PRCs. Similar to the identical PRC case, we achieve a tenfold input power reduction by using the proposed technique (input power decreases from 0.86 to 0.083). However, the baseline technique results in a notable difference of 0.73 rad between the desired and observed phase difference, while the error remains small (0.05 rad) for the proposed algorithm. The increased error for the baseline method can be attributed to the dissimilar oscillator PRCs.

**Case 3 (Heterogeneous PRC):** As illustrated, for heterogeneous PRC oscillators, it becomes imperative to incorporate PRC heterogeneity in the control design process to obtain an accurate phase difference. Neglecting to do so can sometimes result in multiple entrainment phases, depending on the initial phase differences. We empirically substantiated this by entraining a pair of more heterogeneous PRCs in an in-phase configuration where $(\varphi_1^*, \varphi_2^*) = (\pi, \pi)$. The oscillator's natural frequencies are $(0.4475, 0.4505)$ rad/s, and the input frequency is taken as the mean oscillator frequency. The results of our method are displayed in Fig. 3(b3), where we notice that PRC heterogeneity does not influence performance. However, for the baseline method, using the mean PRC for control design results in two stable fixed points for the slower (red) oscillator. These stable fixed points are depicted by the red and light blue colors in the upper-left quadrant of Fig. 3(a3). This implies that the slower oscillator can, indeed,

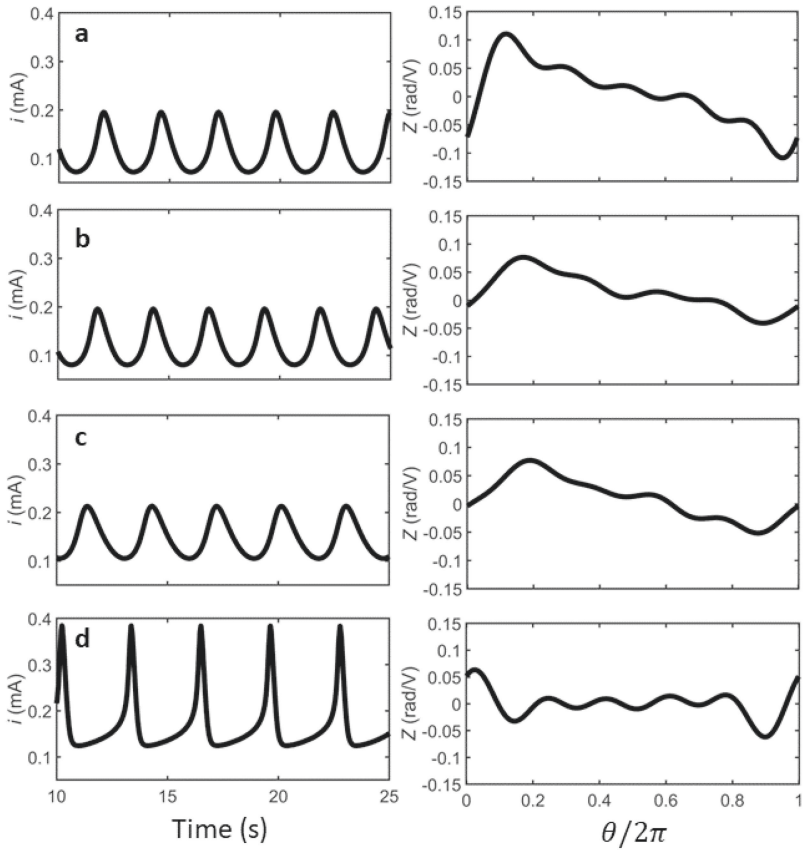


**FIG. 5.** Experiments in the oscillatory nickel electrodissolution: current time series $i(t)$ (left column) and the estimated PRC (right column) of the electrochemical oscillator for different values for circuit potential $V_0$ and individual resistance $R_{ind}$. (a) $(V_0, R_{ind}) = (1090\ \text{mV}, 1\text{k}\Omega)$. (b) $(V_0, R_{ind}) = (1150\ \text{mV}, 1\ \text{k}\Omega)$. (c) $(V_0, R_{ind}) = (1150\ \text{mV}, 1.5\ \text{k}\Omega)$. (d) $(V_0, R_{ind}) = (1250\ \text{mV}, 1\ \text{k}\Omega)$.

entrain at two disparate phases, depending on its initial phase. We observe a similar phenomenon during experiments. The results corresponding to the light blue entrainment phase are shown in Fig. 3(a3), where oscillators are entrained in an anti-phase configuration instead of an in-phase pattern (the other entertainment phase, dark red, results in in-phase entrainment). The proposed technique still generates a smaller power input (input power is reduced to 0.021 compared to the baseline power of 0.158). The comparison of input power and the error in the synchronization patterns for all three cases is displayed in the top panel of Fig. 7.

### 2. Entrainment of oscillator assemblies

Having shown the optimality and robustness to PRC variations of our technique on a pair of oscillators, we now consider cluster formation with four oscillators. Specifically, we form one- and two-cluster states in a group of oscillators with frequencies $(\omega_1, \omega_2, \omega_3, \omega_4) = (0.4453, 0.4475, 0.4505, 0.4536)$ rad/s by designing an input with $\Omega = 0.4492$ rad/s frequency. The entrainment phases are taken as $(\varphi_1^*, \varphi_2^*, \varphi_3^*, \varphi_4^*) = (\pi/2, \pi/2, \pi/2, \pi/2)$ for the one-cluster state, while $(\pi/2, \pi/2, 3\pi/2, 3\pi/2)$ for the two-cluster state. The oscillators denoted by identical colors have identical PRCs; precisely, the red (black) color oscillators have PRC shown in Fig. 1(c). The results of the one-cluster (two-cluster) states are shown in the top (bottom) panel of Fig. 4. For the two-cluster state, we keep the oscillators with identical PRCs in identical clusters.

## B. Experimental results

### 1. PRC estimation

Figure 5 shows the waveform of the current and the PRCs for the different parameters of $V_0$ and $R_{ind}$. As some previous studies have pointed out,[40,51] at $V_0 = 1090$ mV and $R_{ind} = 1$ kΩ, the oscillation waveform is sinusoidal with natural frequency $\omega = 2.16$rad/s and predominantly first harmonic components in the PRC [Fig. 5(a)]. The waveform and the measured PRC are shown in Fig. 5(b) for an increase in the circuit potential ($V_0 = 1150$ mV) while keeping the same $R_{ind} = 1$kΩ. We observed a similar sinusoidal waveform with a natural frequency of $\omega = 2.28$ rad/s. When both the circuit potential and the individual resistance were increased ($V_0 = 1150$ mV, $R_{ind} = 1.5$ kΩ), the waveform was slightly different from those in Figs. 5(a) and 5(b) with $\omega = 2.18$ rad/s. The PRC showed mainly first harmonic [see Fig. 5(c)]. Figure 5(d) illustrates the waveform and the PRC at a higher circuit potential of $V_0 = 1250$ mV and with $R_{ind} = 1$ kΩ. Under these parameters, the oscillations became moderately relaxational with a decrease in the natural frequency to $\omega =$

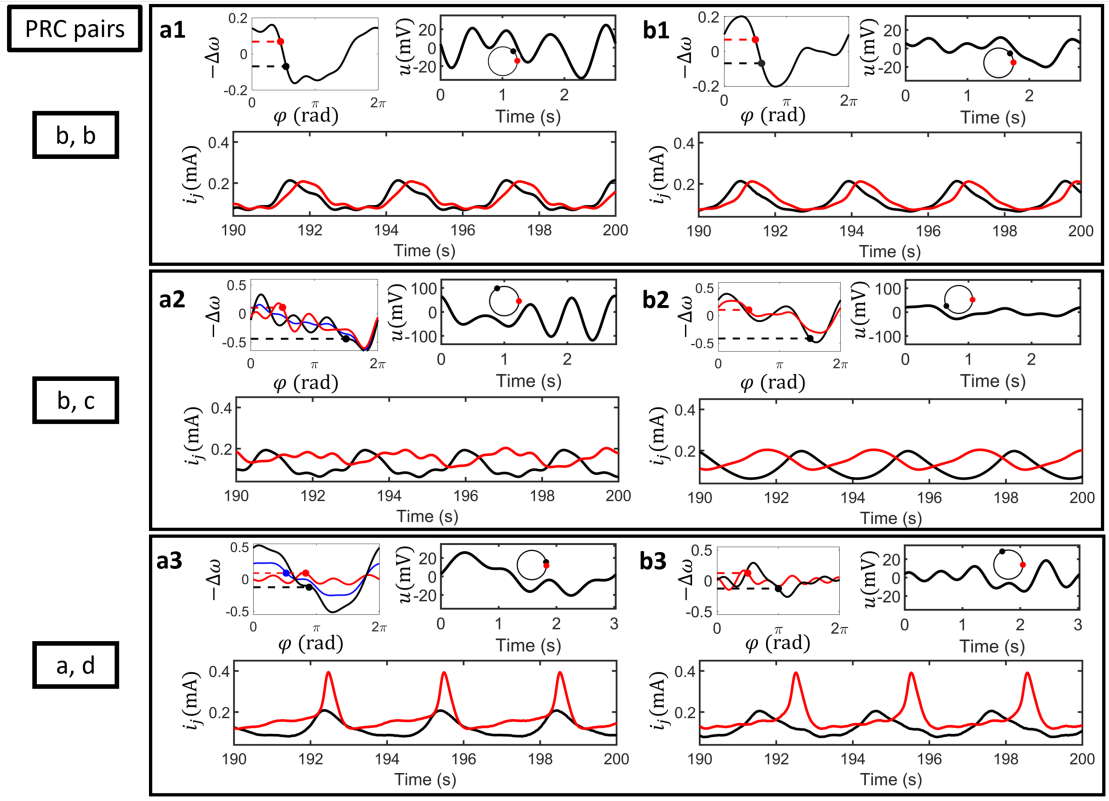


**FIG. 6.** Experiments in the nickel electrodissolution: A comparison of the optimality and robustness against PRC heterogeneity of the baseline method [(a1)–(a3)] and with the proposed technique [(b1)–(b3)]. The top-left, top-right, and bottom figures of each panel depict the designed interaction function, control input, and the time series of the current of each oscillator. The inset panel in the control input shows a snapshot of the phases for each oscillator after reaching a stationary state. The red and black colors correspond to the slower and faster oscillators, respectively. (a1) and (b1), (a2) and (b2), and (a3) and (b3) correspond to three different pairs of PRC depicted in Fig. 5. The blue line in (a2) and (a3) shows the interaction function corresponding to the mean PRC of two oscillators.

2.02 rad/s. At these conditions, the PRC exhibited higher harmonics as the system moved further away from the Hopf bifurcation.

### 2. Phase-selective entrainment of a pair of oscillators

Similar to numerical simulations, we consider three pairs of oscillators, each with different PRC heterogeneities, and entrain them in various phase patterns. The results are shown for in-phase, anti-phase, and out-of-phase in Fig. 6 for all three PRC pairs. For each phase pattern, we determine the interaction function and the control input using the proposed technique and the baseline method. The designed input is then applied to offset circuit potential, and the current ($i_j$) time series of each oscillator is recorded. The corresponding phases of the oscillators are determined from the recorded time series using peak-finding algorithms.[44,53]

**Case 1 (Identical PRC):** To begin, we consider the pair of oscillators with identical PRCs and entrain them in an in-phase configuration by taking $(\varphi_1^*, \varphi_2^*) = (\pi/2, \pi/2)$ using both methods. The oscillator frequencies are $(\omega_1, \omega_2) = (2.15, 2.29)$ rad/s, and the input frequency is taken as the mean of oscillator frequencies. The designed interaction function, control input, and recorded oscillator time series are shown in the top-left, top-right, and bottom parts of Figs. 6(a1) and 6(b1), which correspond to the baseline and proposed method, respectively. We find that the proposed method used three times less power ($P = 8.1 \times 10^{-5}$) than the baseline method ($P = 24.5 \times 10^{-5}$). The time series of experiments in Fig. 6(a1) shows a distorted waveform than those in Fig. 6(b1) as a result of strong forcing. The difference between the designed and observed phase difference is similar for both methods (baseline error: 0.76 rad and the proposed method error: 0.68 rad). The experiments, thus, confirm that with identical PRCs, in-phase synchronized entrained oscillators can be achieved with both methods. These results are consistent with previous experiments[41] and theoretical studies[42] with ensembles of oscillators.

**Case 2 (Marginally heterogeneous PRC):** The anti-phase entrainment of two oscillators with marginally different PRCs [see Figs. 5(b) and 5(c)] is shown in Figs. 6(a2) and 6(b2), where

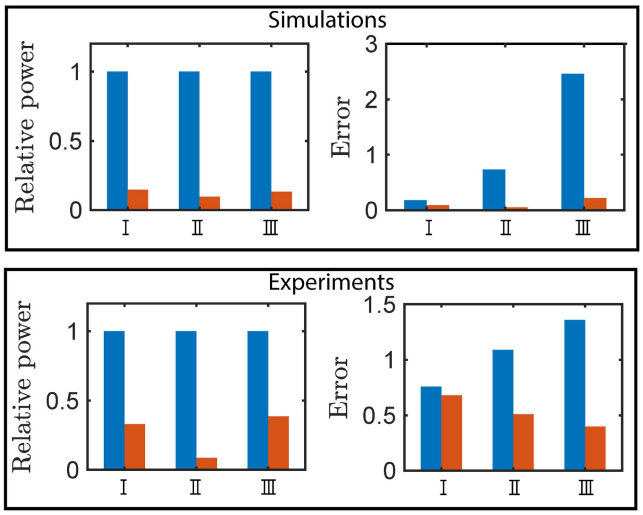


**FIG. 7.** A comparison of input power and the error in the synchronization pattern between the proposed technique and the baseline method for different PRC heterogeneities (I,II, and III); I: a pair of oscillators with identical PRC, II: a pair of oscillators with slightly heterogeneous PRCs, and III: a pair of oscillators with significantly heterogeneous PRCs. The blue and orange color bars indicate the results for the baseline and the proposed method, respectively.

$(\varphi_1^*, \varphi_2^*) = (\pi/2, 3\pi/2)$. The oscillator frequencies are $(\omega_1, \omega_2) = (2.18, 2.68)$ rad/s, and the input frequency is taken as $\Omega = 2.26$ rad/s. For the baseline method, we use the mean PRC to design the interaction function, shown by the blue line in the top-left part of Fig. 6(a2). Similar to the previous case, the control input generated using the proposed method ($P = 24.2 \times 10^{-5}$) uses ten times less power than the baseline input ($P = 280 \times 10^{-5}$). The time series of the recorded currents using the control signal generated by the baseline method shows substantial modifications in the waveform due to more drastic changes in the circuit potential than in the proposed method. In this case, the error is more prominent in the baseline method (1.12 rad) than in the proposed method (0.45 rad). The findings indicate that heterogeneity in the PRCs of the oscillators led to an increase in the error of the designated phase difference when the baseline method is implemented. However, using the suggested approach, the error remained similar for identical and heterogeneous PRCs.

**Case 3 (Heterogeneous PRC):** Figures 6(a3) and 6(b3) show the results when the heterogeneity between the PRCs is further increased. In this case, an out-of-phase ($\pi/2 \approx 1.57$ rad) phase difference is designed by taking $(\varphi_1^*, \varphi_2^*) = (\pi/2, \pi)$. The oscillator frequencies are $(\omega_1, \omega_2) = (1.95, 2.20)$ rad/s, and the input frequency is taken as the mean of the oscillator frequencies. The faster oscillator is close to the Hopf bifurcation, exhibiting a sinusoidal waveform [Fig. 5(a)], while the slower one in a parameter region with a more relaxational characteristic [Fig. 5(d)]. As in the previous

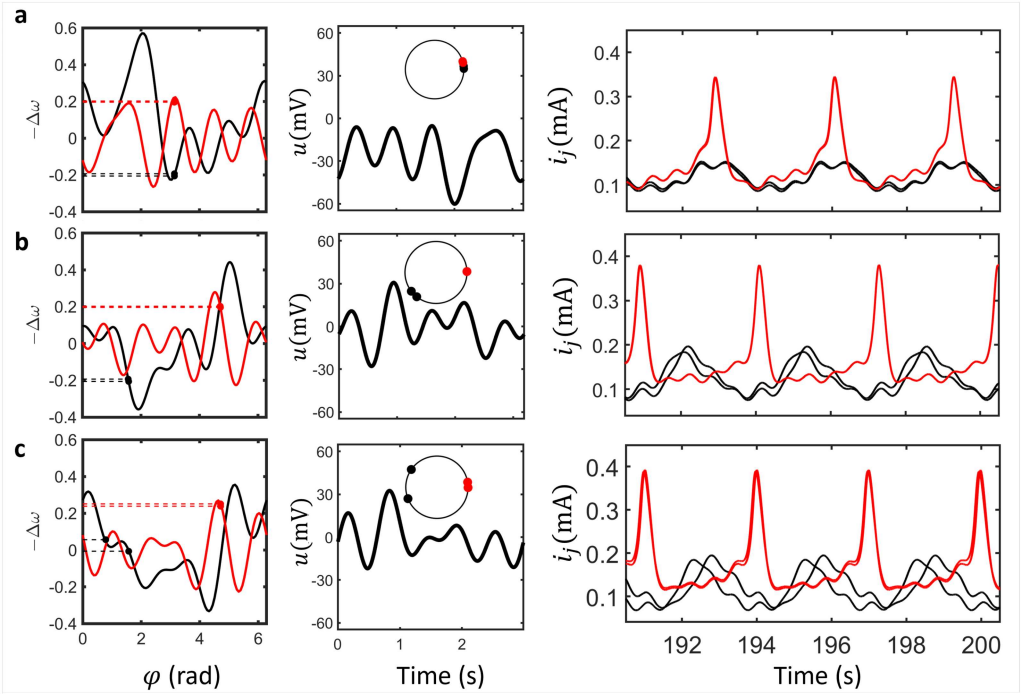


**FIG. 8.** Phase assignment for a population of four oscillators with the proposed method. (a) One-cluster with ($N = 4$) elements. (b) Two-cluster with ($N_1$, $N_2$) = (2, 2) elements. (c) Three-cluster state with ($N_1$, $N_2$, $N_3$) = (1,1,2) elements. For each panel, left to right: interaction function, control input (inset: phases on the unit circle), and the current time series. The red (black) color denotes the slower (faster) oscillators, where oscillators having identical PRC are represented by the same color.

cases, the baseline input has more power ($P = 18 \times 10^{-5}$) than the proposed method ($P = 7 \times 10^{-5}$). However, for such large PRC heterogeneity, we observe that the baseline method entrains the oscillators in an in-phase configuration instead of an out-of-phase pattern. This is because the interaction function is designed based on the mean PRC (blue line), but the actual interaction function (red line) differs from the mean interaction function. As a result, the oscillator entrains to the phase difference shown by the red dot in the top-left portion of Fig. 5(a3). On the other hand, the proposed method entrains the oscillators to a 1.97 rad phase difference with a relatively smaller error of 0.40 rad. This experiment demonstrates that in conditions where the heterogeneities of the PRCs are significant, the assigned phase difference could be quite different than the observed phase difference if the mean PRC is used for the control design.

### 3. Input power and error analysis

The experimental results of the power and error for both methods are compared in Fig. 7 (bottom panel). As we can observe, the relative power of the proposed method was in the interval $P = 0.09$ to 0.39 for the three different phase assignments with different PRC heterogeneities. As PRC heterogeneity increases, the error for the baseline technique increases, from 0.76 to 1.36 rad, while the proposed method remained relatively constant between 0.40 and 0.70 rad, demonstrating robustness against PRC heterogeneity. In addition, the suggested approach consistently generates smaller power inputs for all experiments done in this work.

### 4. Phase-selective entrainment of four oscillators

We also conduct experiments with four oscillators to display cluster formation. Figure 8 shows the one- (top row), two- (middle row), and three-cluster (bottom row) states designed with the proposed algorithm. For the one- and two-cluster states, oscillator frequencies are $(\omega_1, \omega_2, \omega_3, \omega_4) = (2.16, 2.17, 1.77, 1.76)$ rad/s and the input frequency is taken as $\Omega = 1.96$ rad/s; while for the three-cluster state, oscillator frequencies are $(2.04, 2.10, 1.85, 1.86)$ rad/s with the designed input of $\Omega = 2.1$ rad/s. The entrainment phases for one-, two-, and three-cluster states are taken as $(\pi, \pi, \pi, \pi)$, $(3\pi/2, 3\pi/2, \pi/2, \pi/2)$, and $(\pi/4, \pi/2, 3\pi/2, 3\pi/2)$, respectively. Oscillators 1 and 2 are close to Hopf bifurcation and have identical PRC [Fig. 5(a)], while slower oscillators, i.e., oscillators 3 and 4, have identical PRC and display relaxational characteristics [Fig. 5(d)]. For such a heterogeneous population, we find that our technique can successfully obtain the desired cluster configuration, highlighting its experimental applicability to large heterogeneous oscillator populations.

## IV. CONCLUSIONS

Numerical simulations and experimental evidence in the nickel electrodissolution system were presented for optimal entrainment of heterogeneous oscillators. Phase-selective entrainment was applied to heterogeneous oscillators with a global signal. Various entrainments with in-phase, anti-phase, and out-of-phase configurations were demonstrated with different levels of correlations of the PRCs of the oscillator pairs. In addition, the technique was also demonstrated for a set of four oscillators for one-, two-, and three-cluster configurations.

This approach enables entraining oscillators with heterogeneous PRCs, which expands the technique limited to control oscillators with identical PRCs.[41] Our proposed approach transforms the continuous domain control task into a discrete convex quadratic program (QP), which is both computationally efficient and yields a globally optimal signal. This contrasts with the commonly used method for control design via optimal control theory (see Refs. 54–57), which involves solving a set of boundary value differential equations—a process that is computationally intensive and typically results in a locally optimal solution. Additionally, the transformation of the control design problem into a convex QP facilitates scaling to large arrays of oscillators, as the worst-case computational complexity for solving a convex QP is polynomial time with system size, namely, $\mathcal{O}(N^3)$.[58] The main limitations of the method are related to the use of phase models. As the heterogeneity in oscillator frequency increases, stronger inputs are required for phase-selective entrainment. This might invalidate the weak forcing assumption that underpins the validity of phase models. Further investigation is needed to effectively control sufficiently large heterogeneous populations beyond phase models. From an experimental perspective, the relative phase distribution of large oscillator populations can be designed as long as the PRCs and the (natural) frequencies of the oscillators can be measured (or estimated).

The presented control technique consistently used less power in numerical simulations and experiments with oscillatory electrochemical reactions. This feature makes the technique suitable for controlling biological neuronal ensembles, where noninvasive and mild control is desired to fine-tune system behavior without disrupting its fundamental properties. For instance, in medical device development, synchronizing cardiac tissues with low power forcing is crucial for addressing cardiac arrhythmias.[59] Similarly, for the treatment of brain disorders, minimum-power optimal stimuli are required to desynchronize oscillator populations.[33] In addition, our technique does not require real-time feedback and can successfully obtain stable synchronization structures using only the knowledge of the natural frequencies and the PRCs of the population, both of which can be determined from the experimental data.

## ACKNOWLEDGMENTS

I.Z.K. acknowledges the funding from the National Science Foundation under Grant No. CHE-1900011 grant. J.S.L. acknowledges the financial support from under AFOSR Award No. FA9550-21-1-0335.

## DATA AVAILABILITY

The data that support the findings of this study are available from the corresponding author upon reasonable request.

## AUTHOR DECLARATIONS

### Conflict of Interest

The authors have no conflicts to disclose.

## Author Contributions

Jorge Luis Ocampo-Espindola and Bharat Singhal contributed equally to this work.

**Jorge Luis Ocampo-Espindola:** Conceptualization (equal); Formal analysis (equal); Investigation (equal); Writing – original draft (equal); Writing – review & editing (equal). **Bharat Singhal:** Conceptualization (equal); Formal analysis (equal); Investigation (equal); Writing – original draft (equal); Writing – review & editing (equal). **Jr-Shin Li:** Conceptualization (equal); Writing – original draft (equal); Writing – review & editing (equal). **István Z. Kiss:** Conceptualization (equal); Writing – review & editing (equal).

## REFERENCES


[1]S. H. Strogatz, *Nonlinear Dynamics and Chaos: With Applications to Physics, Biology, Chemistry, and Engineering*, 2nd edition (CRC Press, 2018).
[2]A. T. Winfree, *The Geometry of Biological Time* (Springer New York, New York, 2001), pp. 545–591.
[3]I. R. Epstein and J. A. Pojman, "An introduction to nonlinear chemical dynamics: Oscillations, waves, patterns, and chaos," in *Topics in Physical Chemistry* (Oxford University Press, 1998).
[4]A. K. Engel, P. Fries, and W. Singer, "Dynamic predictions: Oscillations and synchrony in top–down processing," Nat. Rev. Neurosci. **2**, 704–716 (2001).
[5]A. Schnitzler and J. Gross, "Normal and pathological oscillatory communication in the brain," Nat. Rev. Neurosci. **6**, 285–296 (2005).
[6]E. Rodriguez, N. George, J.-P. Lachaux, J. Martinerie, B. Renault, and F. J. Varela, "Perception's shadow: Long-distance synchronization of human brain activity," Nature **397**, 430–433 (1999).
[7]P. J. Uhlhaas and W. Singer, "Neural synchrony in brain disorders: Relevance for cognitive dysfunctions and pathophysiology," Neuron **52**, 155–168 (2006).
[8]K. Lehnertz, S. Bialonski, M.-T. Horstmann, D. Krug, A. Rothkegel, M. Staniek, and T. Wagner, "Synchronization phenomena in human epileptic brain networks," J. Neurosci. Methods **183**, 42–48 (2009).
[9]C. Rummel, M. Goodfellow, H. Gast, M. Hauf, F. Amor, A. Stibal, L. Mariani, R. Wiest, and K. Schindler, "A systems-level approach to human epileptic seizures," Neuroinformatics **11**, 159–173 (2013).
[10]S. Ahn, C. Park, and L. L. Rubchinsky, "Neural synchronization in Parkinson's disease on different time scales," in *Multiscale Models of Brain Disorders* (Springer International Publishing, Cham, 2019), pp. 57–65.
[11]C. Hammond, H. Bergman, and P. Brown, "Pathological synchronization in Parkinson's disease: Networks, models and treatments," Trends Neurosci. **30**, 357–364 (2007).
[12]V. Petrov, V. Gáspár, J. Masere, and K. Showalter, "Controlling chaos in the Belousov—Zhabotinsky reaction," Nature **361**, 240–243 (1993).
[13]I. Z. Kiss, C. G. Rusin, H. Kori, and J. L. Hudson, "Engineering complex dynamical structures: Sequential patterns and desynchronization," Science **316**, 1886–1889 (2007).
[14]I. Z. Kiss, "Synchronization engineering," Curr. Opin. Chem. Eng. **21**, 1–9 (2018).
[15]C. G. Rusin, H. Kori, I. Z. Kiss, and J. L. Hudson, "Synchronization engineering: Tuning the phase relationship between dissimilar oscillators using nonlinear feedback," Philos. Trans. R. Soc., A **368**, 2189–2204 (2010).
[16]Y. Zhai, I. Z. Kiss, and J. L. Hudson, "Control of complex dynamics with time-delayed feedback in populations of chemical oscillators: Desynchronization and clustering," Ind. Eng. Chem. Res. **47**, 3502–3514 (2008).
[17]M. G. Rosenblum and A. S. Pikovsky, "Controlling synchronization in an ensemble of globally coupled oscillators," Phys. Rev. Lett. **92**, 114102 (2004).
[18]H. Kori, C. G. Rusin, I. Z. Kiss, and J. L. Hudson, "Synchronization engineering: Theoretical framework and application to dynamical clustering," Chaos **18**, 026111 (2008).
[19]C. Bick, M. Sebek, and I. Z. Kiss, "Robust weak chimeras in oscillator networks with delayed linear and quadratic interactions," Phys. Rev. Lett. **119**, 168301 (2017).
[20]M. R. Tinsley, S. Nkomo, and K. Showalter, "Chimera and phase-cluster states in populations of coupled chemical oscillators," Nat. Phys. **8**, 662–665 (2012).
[21]A. M. Hagerstrom, T. E. Murphy, R. Roy, P. Hövel, I. Omelchenko, and E. Schöll, "Experimental observation of chimeras in coupled-map lattices," Nat. Phys. **8**, 658–661 (2012).
[22]E. Boyers, M. Pandey, D. K. Campbell, A. Polkovnikov, D. Sels, and A. O. Sushkov, "Floquet-engineered quantum state manipulation in a noisy qubit," Phys. Rev. A **100**, 012341 (2019).
[23]J.-S. Li, J. Ruths, T.-Y. Yu, H. Arthanari, and G. Wagner, "Optimal pulse design in quantum control: A unified computational method," Proc. Natl. Acad. Sci. U.S.A. **108**, 1879–1884 (2011).
[24]P. A. Tass, *Phase Resetting in Medicine and Biology: Stochastic Modelling and Data Analysis* (Springer Science & Business Media, 2007).
[25]P. A. Tass, "Desynchronizing double-pulse phase resetting and application to deep brain stimulation," Biol. Cybern. **85**, 343–354 (2001).
[26]P. Tass, "Effective desynchronization by means of double-pulse phase resetting," Europhys. Lett. **53**, 15 (2001).
[27]P. A. Tass, "Effective desynchronization with bipolar double-pulse stimulation," Phys. Rev. E **66**, 036226 (2002).
[28]P. Tass, "Effective desynchronization with a resetting pulse train followed by a single pulse," Europhys. Lett. **55**, 171 (2001).
[29]P. Tass, "Effective desynchronization with a stimulation technique based on soft phase resetting," Europhys. Lett. **57**, 164 (2002).
[30]W. B. Bomela, I. S. Dasanayake, J.-S. Li, Y. Chen, and I. Z. Kiss, "Optimal phase-to-phase control of chemical oscillations," Ind. Eng. Chem. Res. **57**, 7764–7770 (2018).
[31]A. Nabi and J. Moehlis, "Time optimal control of spiking neurons," J. Math. Biol. **64**, 981–1004 (2012).
[32]W. Bomela, B. Singhal, and J.-S. Li, "Engineering spatiotemporal patterns: Information encoding, processing, and controllability in oscillator ensembles," Biomed. Phys. Eng. Exp. **9**, 045033 (2023).
[33]D. Wilson and J. Moehlis, "Optimal chaotic desynchronization for neural populations," SIAM J. Appl. Dyn. Syst. **13**, 276 (2014).
[34]A. Zlotnik and J.-S. Li, "Optimal entrainment of neural oscillator ensembles," J. Neural Eng. **9**, 046015 (2012).
[35]D. Wilson and J. Moehlis, "An energy-optimal approach for entrainment of uncertain circadian oscillators," Biophys. J. **107**, 1744–1755 (2014).
[36]K. M. Stiefel, B. S. Gutkin, and T. J. Sejnowski, "Cholinergic neuromodulation changes phase response curve shape and type in cortical pyramidal neurons," PLoS One **3**, e3947 (2008).
[37]Y. Tsubo, M. Takada, A. D. Reyes, and T. Fukai, "Layer and frequency dependencies of phase response properties of pyramidal neurons in rat motor cortex," Eur. J. Neurosci. **25**, 3429–3441 (2007).
[38]S. D. Burton, G. B. Ermentrout, and N. N. Urban, "Intrinsic heterogeneity in oscillatory dynamics limits correlation-induced neural synchronization," J. Neurophysiol. **108**, 2115–2133 (2012).
[39]D. Morse, J. W. Hastings, and T. Roenneberg, "Different phase responses of the two circadian oscillators in Gonyaulax," J. Biol. Rhythms **9**, 263–274 (1994).
[40]I. Z. Kiss, Y. Zhai, and J. L. Hudson, "Predicting mutual entrainment of oscillators with experiment-based phase models," Phys. Rev. Lett. **94**, 248301 (2005).
[41]A. Zlotnik, R. Nagao, I. Z. Kiss, and J.-S. Li, "Phase-selective entrainment of nonlinear oscillator ensembles," Nat. Commun. **7**, 10788 (2016).
[42]B. Singhal, I. Z. Kiss, and J.-S. Li, "Optimal phase-selective entrainment of heterogeneous oscillator ensembles," SIAM J. Appl. Dyn. Syst. **22**, 2180–2205 (2023).
[43]H. Nakao, "Phase reduction approach to synchronisation of nonlinear oscillators," Contemp. Phys. **57**, 188–214 (2016).
[44]A. Pikovsky, M. Rosenblum, and J. Kurths, "Synchronization—A universal concept in nonlinear sciences," in *Cambridge Nonlinear Science Series* (Cambridge University Press, 2001), Vol. 12, pp. 1–411.
[45]R. Cestnik and M. Rosenblum, "Inferring the phase response curve from observation of a continuously perturbed oscillator," Sci. Rep. **8**, 13606 (2018).
[46]T. Netoff, M. A. Schwemmer, and T. J. Lewis, "Experimentally estimating phase response curves of neurons: Theoretical and practical issues," in *Phase Response*

*Curves in Neuroscience: Theory, Experiment, and Analysis* (Springer New York, NY, 2012), pp. 95–129.
[47]D. Yengi, M. R. Tinsley, and K. Showalter, "Autonomous cycling between excitatory and inhibitory coupling in photosensitive chemical oscillators," Chaos **28**, 045114 (2018).
[48]D. Haim, O. Lev, L. Pismen, and M. Sheintuch, "Modeling periodic and chaotic dynamics in anodic nickel dissolution," J. Phys. Chem. **96**, 2676–2681 (1992).
[49]M. T. Koper, *Advances in Chemical Physics* (John Wiley & Sons, Ltd, 1996), pp. 161–298.
[50]I. Z. Kiss, L. N. Pelster, M. Wickramasinghe, and G. S. Yablonsky, "Frequency of negative differential resistance electrochemical oscillators: Theory and experiments," Phys. Chem. Chem. Phys. **11**, 5720 (2009).
[51]T. Harada, H.-A. Tanaka, M. J. Hankins, and I. Z. Kiss, "Optimal waveform for the entrainment of a weakly forced oscillator," Phys. Rev. Lett. **105**, 088301 (2010).
[52]A. Zlotnik, Y. Chen, I. Z. Kiss, H.-A. Tanaka, and J.-S. Li, "Optimal waveform for fast entrainment of weakly forced nonlinear oscillators," Phys. Rev. Lett. **111**, 024102 (2013).
[53]N. Mitrou, A. Laurin, T. Dick, and J. Inskip, "A peak detection method for identifying phase in physiological signals," Biomed. Signal Process. Control **31**, 452–462 (2017).
[54]D. Wilson and J. Moehlis, "Locally optimal extracellular stimulation for chaotic desynchronization of neural populations," J. Comput. Neurosci. **37**, 243–257 (2014).
[55]D. Wilson, "Optimal open-loop desynchronization of neural oscillator populations," J. Math. Biol. **81**, 25–64 (2020).
[56]B. Monga and J. Moehlis, "Optimal phase control of biological oscillators using augmented phase reduction," Biol. Cybern. **113**, 161–178 (2019).
[57]T. D. Matchen and J. Moehlis, "Phase model-based neuron stabilization into arbitrary clusters," J. Comput. Neurosci. **44**, 363–378 (2018).
[58]Y. Ye and E. Tse, "An extension of Karmarkar's projective algorithm for convex quadratic programming," Math. Program. **44**, 157–179 (1989).
[59]S. Luther, F. H. Fenton, B. G. Kornreich, A. Squires, P. Bittihn, D. Hornung, M. Zabel, J. Flanders, A. Gladuli, L. Campoy, and E. M. Cherry, "Low-energy control of electrical turbulence in the heart," Nature **475**, 235–239 (2011).